Supplemental Figure 1

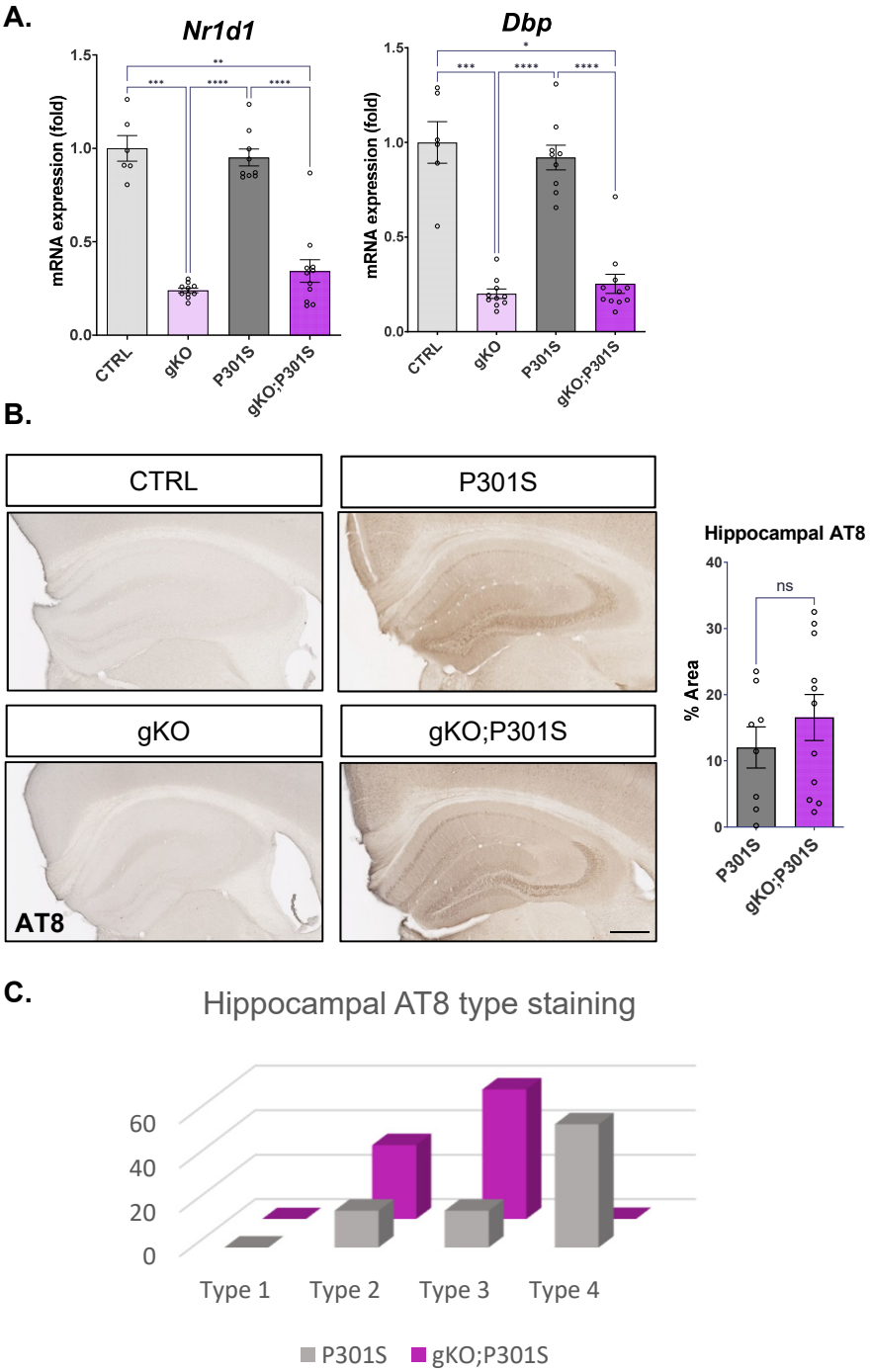

Supplemental Figure 1: Transcriptional changes and tau pathology following global *Bmal1* deletion in P301S mice, related to Figure 1. (A) Decreased expression of the BMAL1 transcriptional targets *Nr1d1* and *Dbp* in gKO and gKO;P301S mouse cortex indicate functional BMAL1 knockout. Main effect of genotype was significant by 2-way ANOVA, and **p<0.01, ***<0.005, ****<0.001 by Sidak's multiple comparison test. (B) ATG staining in hippocampal sections from all four groups of mice form Fig. 1, with quantification of % area of ATG immunoreactivity. Scale bar = 500μm. C. Scoring of degree of tau pathology in mice from Fig. 1, based on the method of Shi Y et al, 2018[17]. Type 1 is minimal pathology, while type 4 encompasses severe tau aggregation and some hippocampal atrophy.

Supplemental Figure 2

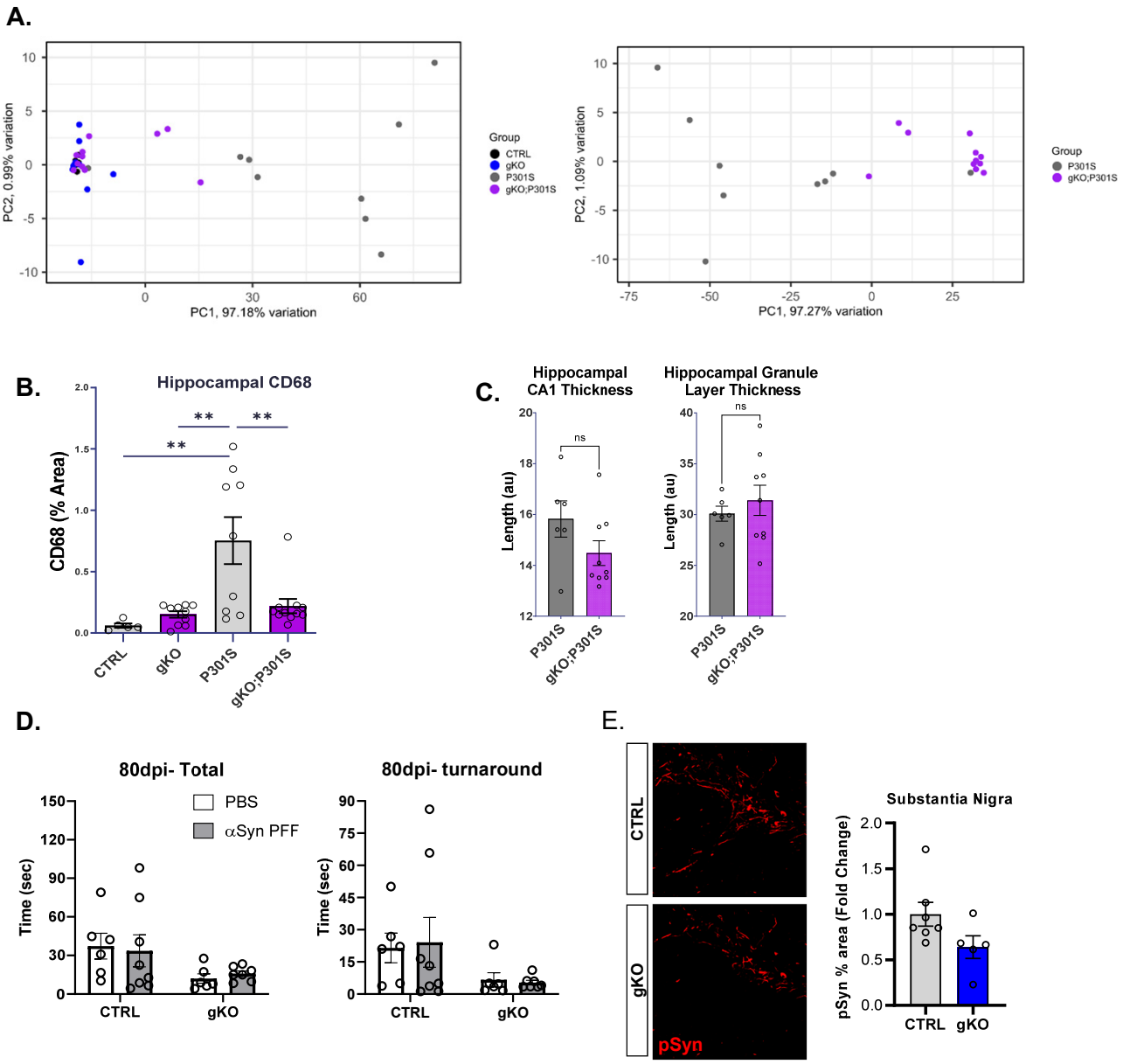

Supplemental Figure 2: Global *Bmal1* deletion suppresses inflammation in P301S mice but does not alter hippocampal degeneration, pole climb behavior, or SNpc αSyn pathology, related to Figure 2. (A) Principal component analysis (PCA) of the inflammatory qPCR panel shown in Figure 2a. (B) Hippocampal CD68 immunofluorescence in all four groups of mice form Fig. 1. Main effect of tau genotype was significant. **P<0.01 by 2-way ANOVA with Sidak's multiple comparisons test. (C) Measurement of thickness of hippocampal CA1 and dentate gyrus granule cell layer in P301S vs. gKO;P301S mice, as assessed by NeuN staining. NS=p>0.1 by 2-tailed T-test. (D) Behavioral data showing the time of total pole climb (left) and time to turnaround (right) for CTRL and gKO mice tested 80 days after PFF injection. No main effects were significant by 2-way ANOVA. (E) pSyn immunofluorescence in the substantia nigra pars compact (SNpc) of CTRL and gKO mice 3 months after PFF injection. For all graphs, one circle represent one mouse, mean±SEM is shown. Scale bar=50μm.

Supplemental Figure 3

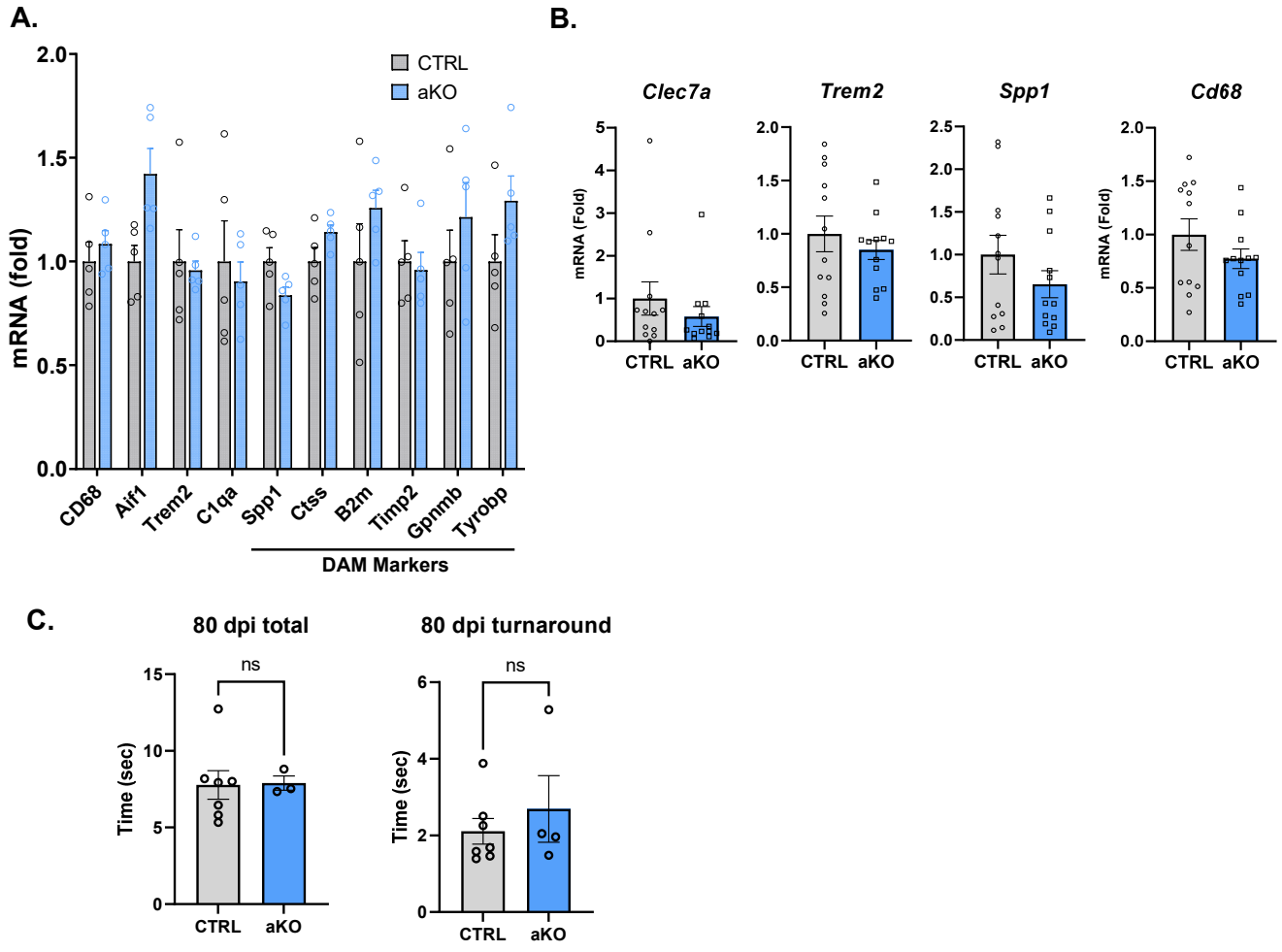

Supplemental Figure 3: Microglial gene expression and pole climb behavioral data in aKO mice, related to Figure 4. (A) Transcript levels of selected microglial activation genes in bulk cortex tissue from adult CTRL and aKO mice 5 months after tamoxifen treatment. The main effect of genotype was significant ($F(1, 80)=4.469$, $P=0.0376$) by 2-way ANOVA, but no individual transcripts were significantly different (CRTL vs. aKO) by Sidak's multiple comparison test. Data is from a previously-published RNAseq experiment {McKee, 2022 #1554}. (B) Selected microglial activation transcript levels in bulk cortex tissue on P301S and aKO;P301S mice, measured by qPCR. All p values were >0.02 by 2-tailed T-test. (C) Behavioral data showing the time of total pole climb (left) and time to turnaround (right) for CTRL and aKO mice tested 80 days after PFF injection. NS= p>0.01 by 2-tailed T-test. For all graphs, one circle represent one mouse, mean±SEM is shown. For A and B, data is expressed as fold change normalized to the mean for the CTRL condition for each transcript.

Supplemental Figure 4

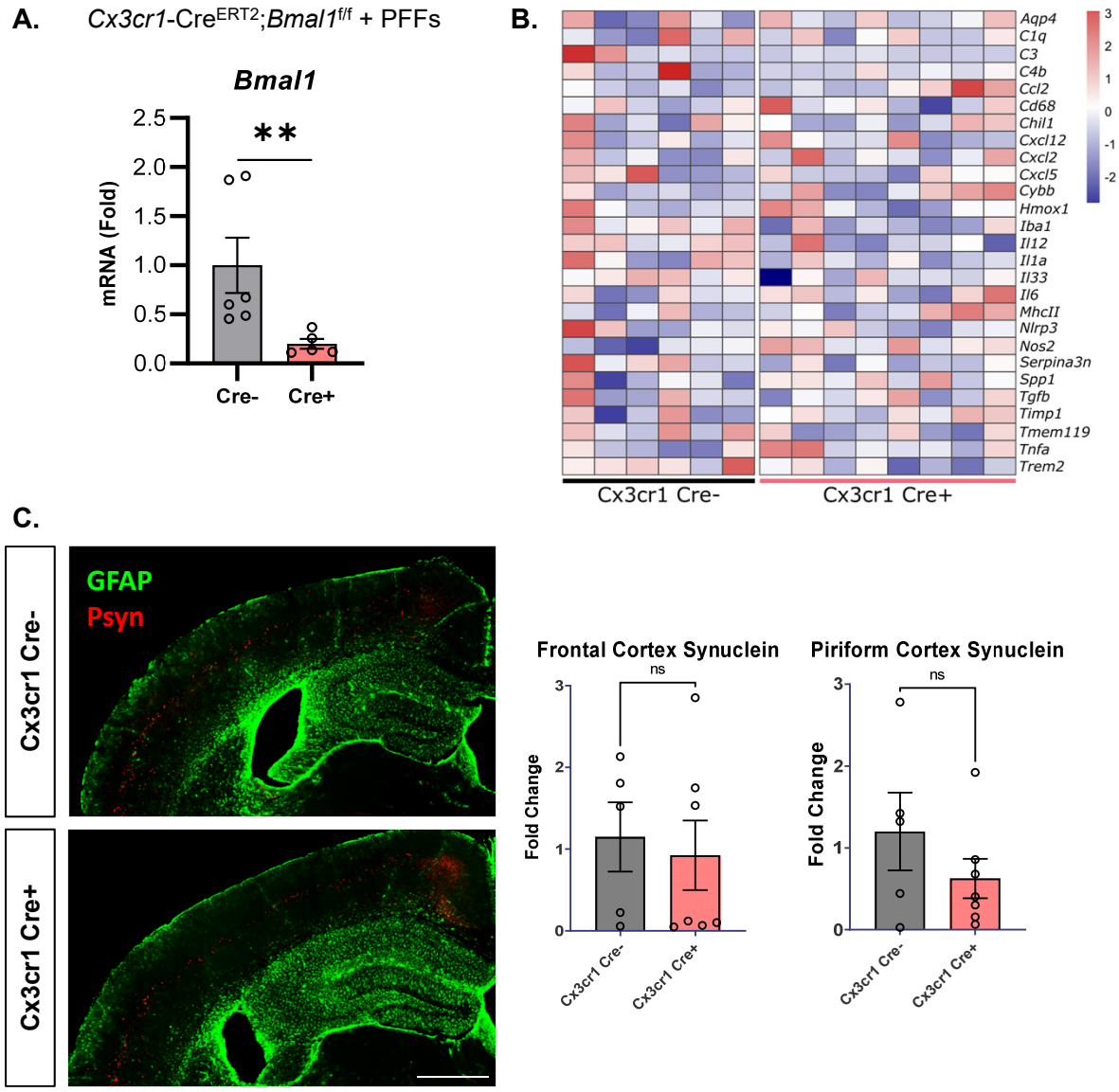

Supplemental Figure 4: Microglial *Bmal1* deletion does not impact α-syn pathology, related to Figure 5. (A) *Cx3cr1*-Cre^{ERT2}; *Bmal1*$^{f/f}$ and Cre-; *Bmal1*$^{f/f}$ littermate controls were treated with tamoxifen at 2mo. One month later, microglia were isolated from using MACS CD11b magnetic beads. *Bmal1* mRNA levels were quantified by qPCR, demonstrating microglial *Bmal1* deletion in Cre+ mice. (B) Microglial activation and DAM transcripts were analyzed via qPCR in bulk cortex tissue from Cx3cr1-Cre^{ERT2}; *Bmal1*$^{f/f}$ and Cre-; *Bmal1*$^{f/f}$ littermate controls. None of the selected genes were significantly differentially expressed. C. Cx3cr1-Cre^{ERT2}; *Bmal1*$^{f/f}$ and Cre-; *Bmal1*$^{f/f}$ littermate controls were treated with tamoxifen at 2 mo, then recieved intrastriatal α-syn PFF injection at 3mo. Mice were then harvested at 6mo., and pSyn immunofluorescence was quantified in frontal and piriform cortex. **p<0.01 by Mann-Whitney U test. In (C), NS = p>0.1 by 2-tailed T-test. Scale bar= 200μm.

Supplemental Figure 5

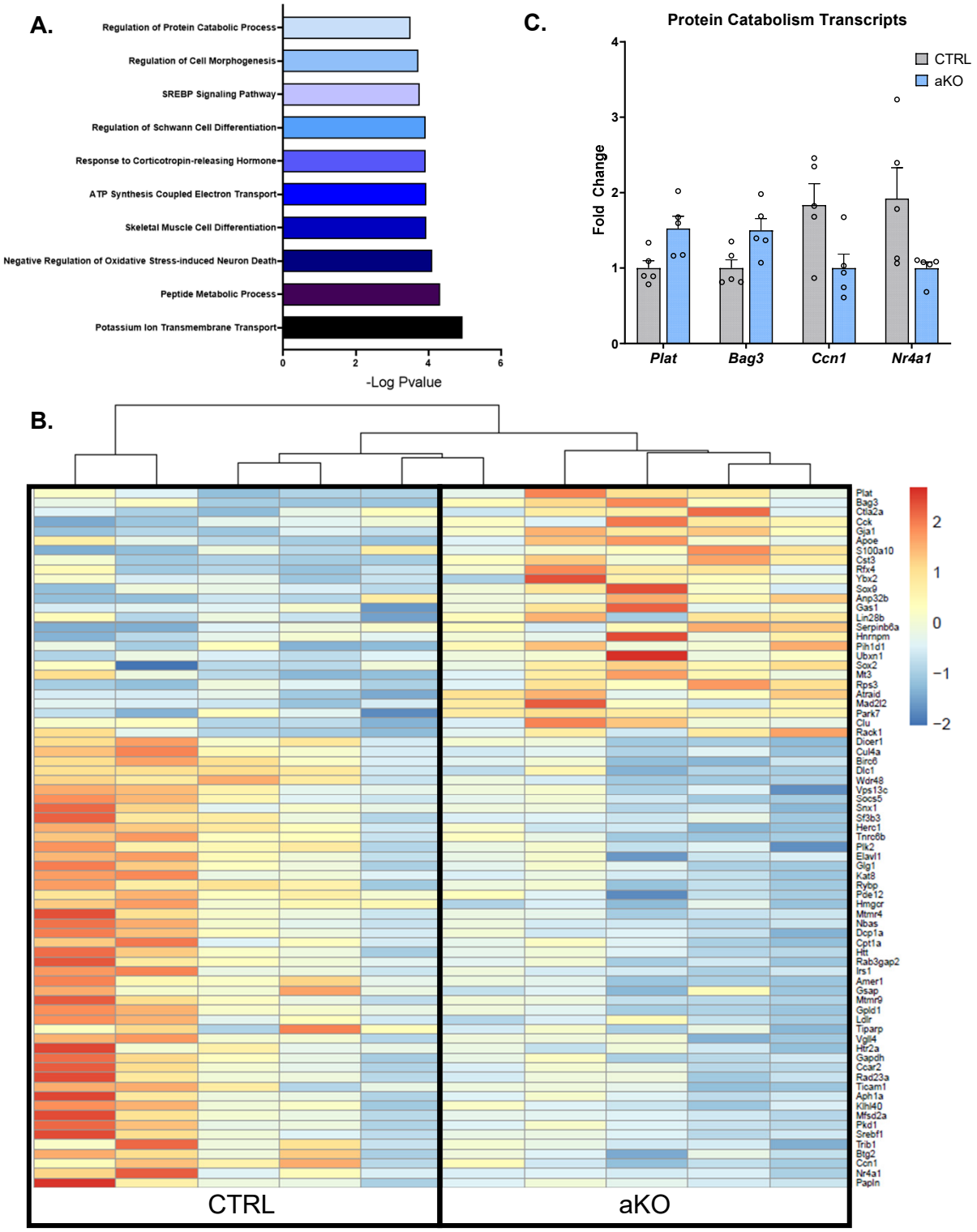

Supplemental Figure 5: Transcriptomic analysis identifies protein catabolism pathway and *Bag3* in aKO brain, related to Figure 6. A. GO term analysis of RNAseq data from McKee et al, *Sci Rep*, 2022. Top 10 pathways are listed. B. Heatmap depicting expression of 71 transcripts comprising the "Regulation of Protein Catabolism". Color indicates Z-score for each row, with warmer colors indicating upregulation. (C) Graph depicting expression of the 4 most significant transcripts from B.

Supplemental Figure 6

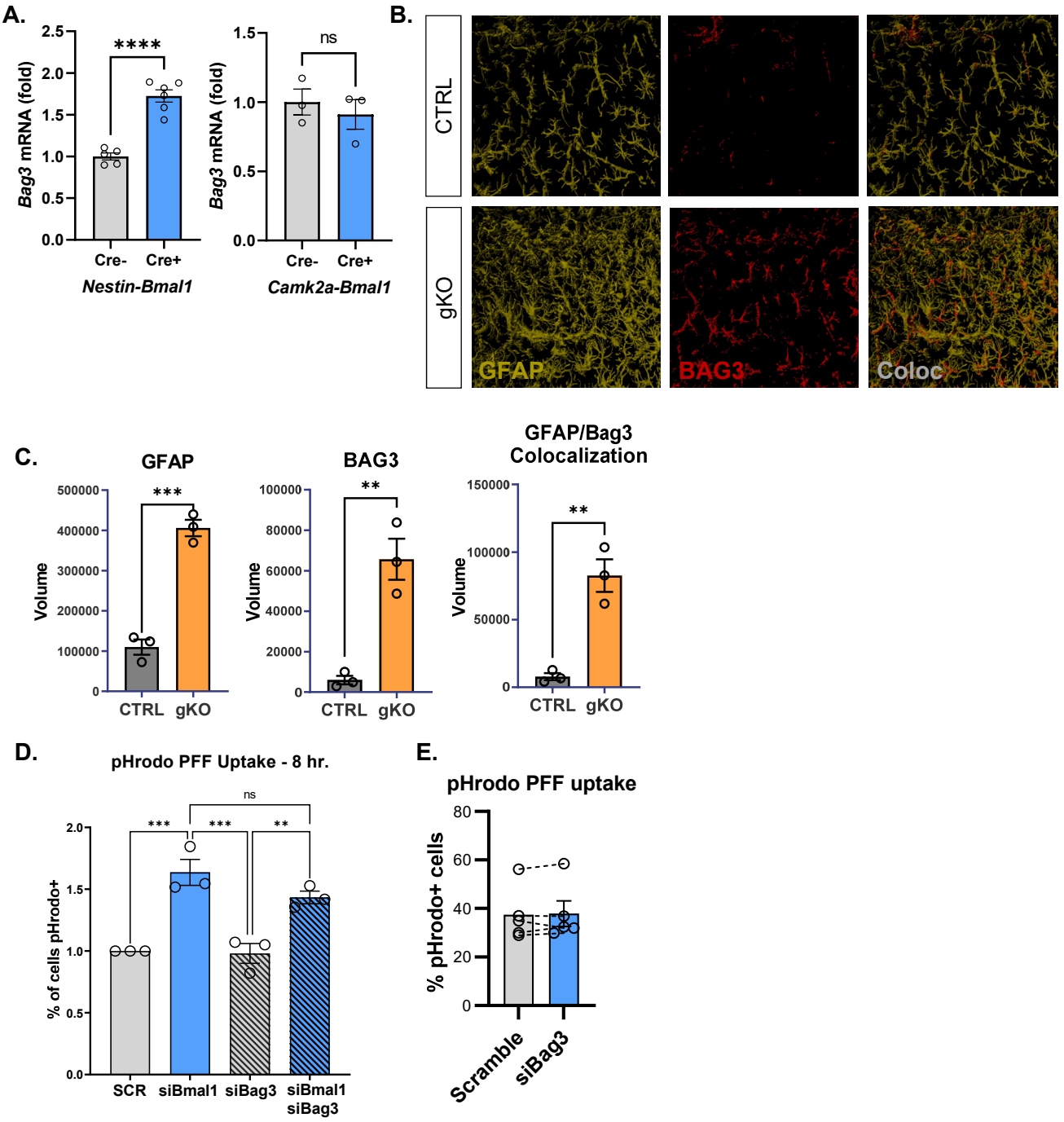

Supplemental Figure 6: BAG3 in gKO mice, related to Figure 6. (A) *Bag3* expression in different *Bmal1* KO mouse lines. All samples were from cerebral cortex. *Nestin*-Cre;*Bmal1*$^{f/f}$ mice have deletion in neurons and glia; *Camk2a*-iCre; *Bmal1*$^{f/f}$ mice have pan-neuronal deletion, as described in Lananna, 2018 #1323. (B) 3D confocal reconstruction images on GFAP and BAG3 immunofluorescence in CTRL and gKO mouse hippocampus, with voxel volume and colocalized volume quantified in (C). (D) pHrodo signal in siRNA-treated astrocyte cultures as in Fig.6h, but this time cells were harvested 8 hours after PFF were washed off (as opposed to 24 hours after in Fig. 6h). (E) pHrodo PFF uptake in astrocyte treated with siBag3 alone as in Fig. 6h. Each circle represent data from an independent experiment. For A and B, each circle represents data from one mouse. **p<0.01, ***<0.005, ****<0.0001 by 2-tailed t-test. For D, p values are the same but derived from 1-way ANOVA.

Supplemental Figure 7

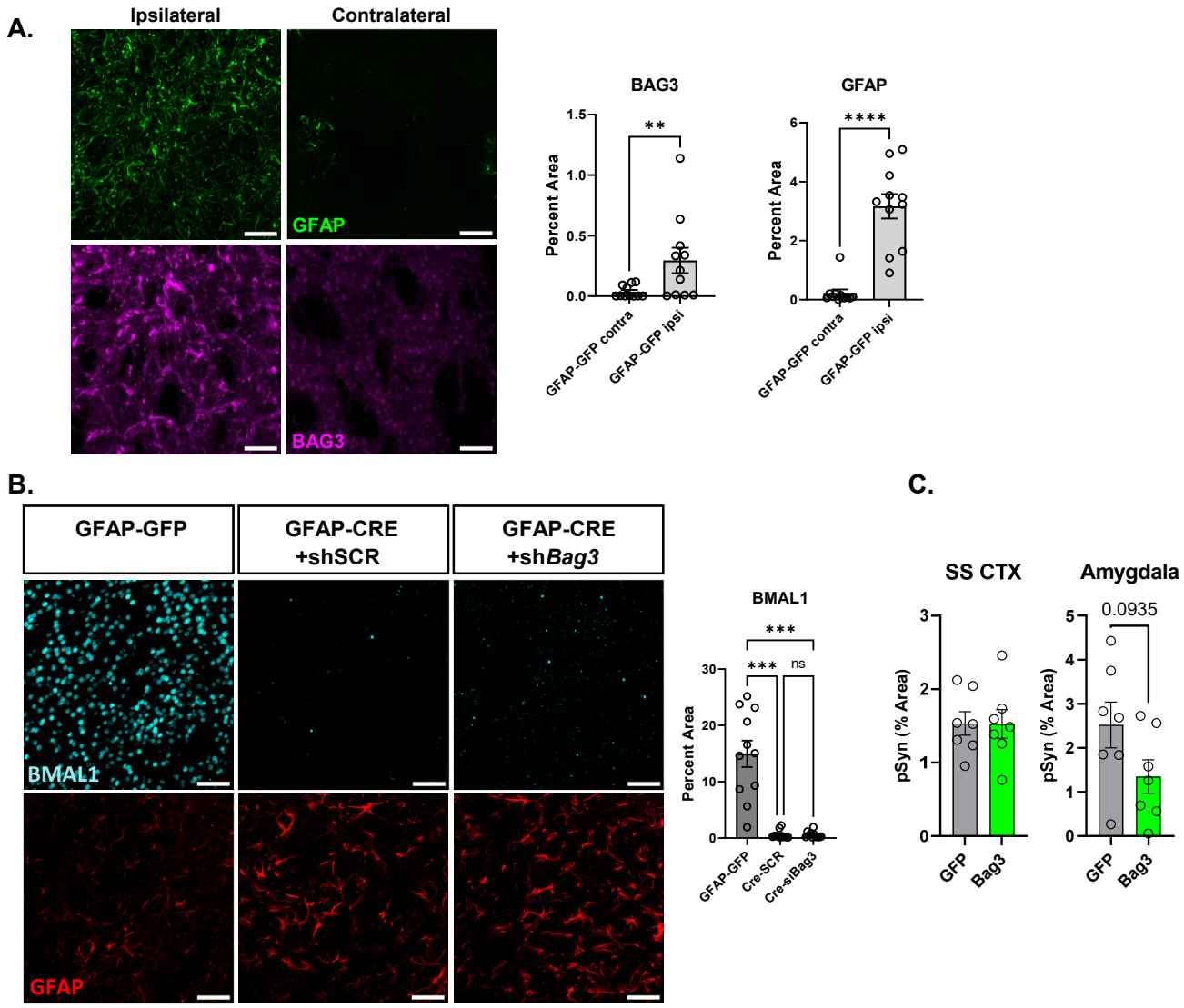

Supplemental Figure 7: BAG3 is induced by stereotactic injection, related to Figure 7. (A) Representative images and quantification of GFAP and BAG3 immunofluorescence in the ipsilateral vs. contralateral striatum in mice from Fig. 7b which were injected unilaterally with control virus (AAV-GFAP-GFP). **p<0.01, ****p<0.0001 by Mann-Whitney U test. (B) Representative images and quantification of BMAL1 and GFAP immunofluorescence in ipsilateral striatum from mice in Fig. 7b. ***p<0.001 by Kruskal-Wallis test with Dunn's multiple comparisons test. (C) pSyn burden in somatosensory cortex (SS CTX) and amygdala from mice from Fig. 7c-e. P value is noted from 2-tailed T-test.

Supplemental Figure 8

A.

	ROSMAP		Knight ADRC		MSBB*		Mayo	
	AD	Control	AD	Control	AD	Control	AD	Control
# Subjects	107	103	68	12	188	35	72	57
AOD (yrs)	88.04	84.39	84.07	90.9	84.62	81.23	82.23	82.28
%APOE4	49.53	11.34	61.76	0	17.02	20	51.39	14.03
% Female	69.07	61.86	54.41	80	68.09	68.57	59.72	43.86

B.

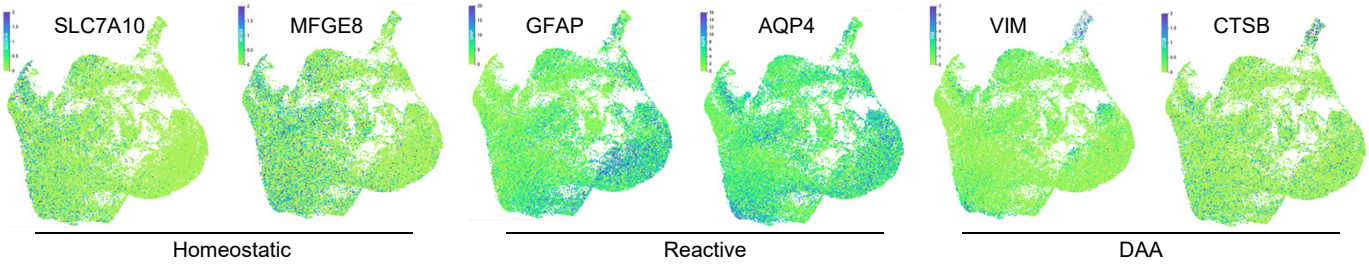

C.

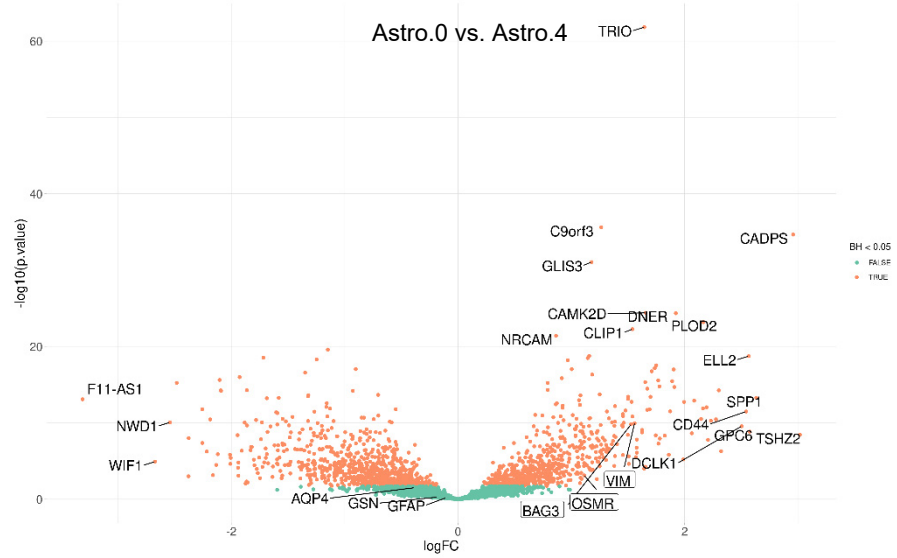

Supplemental Figure 8: *BAG3* is expressed in human astrocytes in human AD, related to Figure 8. (A) Number of brain samples and demographic information from AD cohorts shown in Fig. 8a. (B) Astrocyte cluster from Fig. 8d showing expression of homestatic, reactive, and DAA transcripts, (http://ngi.pub/SNARE/). (D) Volcano plot showing differentially-regulated transcripts between Astro.0 and Astro.4. BAG3 is noted by a box. (E) PD GWAS browser (https://pdgenetics.shinyapps.io/GWASBrowser/) shows SNPs associated with PD risk in *BAG3* intronic regions.

Supplemental Figure 9

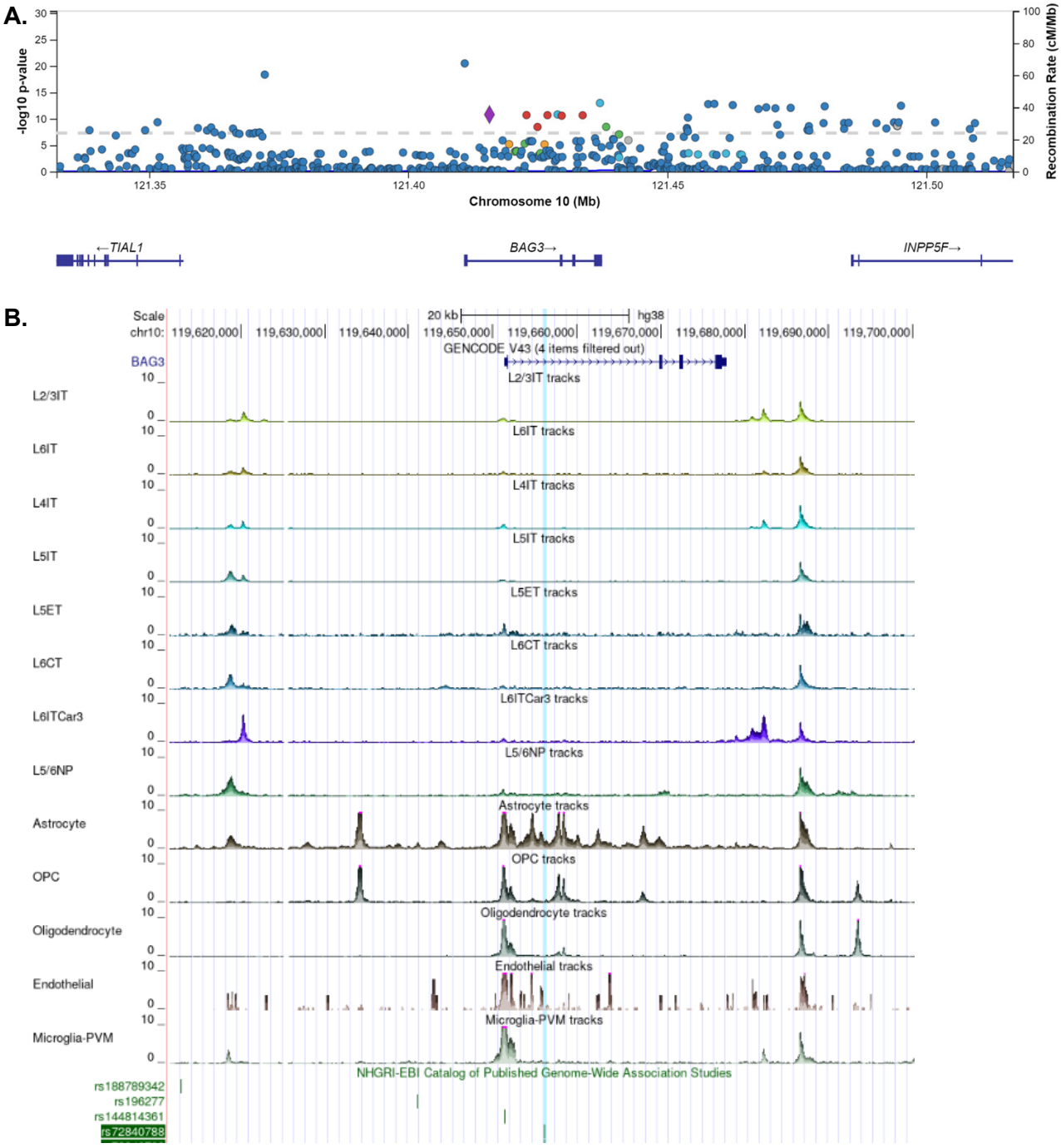

Supplemental Figure 9: *BAG3* is a human PD GWAS hit and a disease-associated SNP is expressed in astrocytes, related to Figure 8. (A) PD GWAS browser (https://pdgenetics.shinyapps.io/GWASBrowser/) shows SNPs associated with PD risk in *BAG3* intronic regions. (B) Single nucleus ATAC-seq data from the SEA-AD cohort in the UCSC Genome Browser for the SNP, rs72840788, a SNP associated with PD risk, shows epression in astrocytes. (https://genome.ucsc.edu/cgi-bin/hgTracks?db=hg38&lastVirtModeType=default&lastVirtModeExtraState=&virtModeType=default&virtMode=0&nonVirtPosition=&position=chr10%3A119611507%2D119700839&hgsid=1591068627_uBIAFTnXpvAgq6jH2Av9lwOidw92).

Table S1: AD Knowledge Portal Full Acknowledgement Information, related to STAR Methods.

The results published in Fig. 8a and Supplemental Fig. 8 are in whole or in part based on data obtained from the AD Knowledge Portal (https://adknowledgeportal.org). The Mayo RNAseq study data was led by Dr. Nilüfer Ertekin-Taner, Mayo Clinic, Jacksonville, FL as part of the multi-PI U01 AG046139 (MPIs Golde, Ertekin-Taner, Younkin, Price). Samples were provided from the following sources: The Mayo Clinic Brain Bank. Data collection was supported through funding by NIA grants P50 AG016574, R01 AG032990, U01 AG046139, R01 AG018023, U01 AG006576, U01 AG006786, R01 AG025711, R01 AG017216, R01 AG003949, NINDS grant R01 NS080820, CurePSP Foundation, and support from Mayo Foundation. Study data includes samples collected through the Sun Health Research Institute Brain and Body Donation Program of Sun City, Arizona. The Brain and Body Donation Program is supported by the National Institute of Neurological Disorders and Stroke (U24 NS072026 National Brain and Tissue Resource for Parkinsons Disease and Related Disorders), the National Institute on Aging (P30 AG19610 Arizona Alzheimers Disease Core Center), the Arizona Department of Health Services (contract 211002, Arizona Alzheimers Research Center), the Arizona Biomedical Research Commission (contracts 4001, 0011, 05-901 and 1001 to the Arizona Parkinson's Disease Consortium) and the Michael J. Fox Foundation for Parkinsons Research. In addition, additional data was generated from postmortem brain tissue collected through the Mount Sinai VA Medical Center Brain Bank and were provided by Dr. Eric Schadt from Mount Sinai School of Medicine, and was accessed via the AD Knowledge Portal. Additional study data was generated from postmortem brain tissue provided by the Religious Orders Study and Rush Memory and Aging Project (ROSMAP) cohort at Rush Alzheimer’s Disease Center, Rush University Medical Center, Chicago. This work was funded by NIH grants U01AG061356 (De Jager/Bennett), RF1AG057473 (De Jager/Bennett), and U01AG046152 (De Jager/Bennett) as part of the AMP-AD consortium, as well as NIH grants R01AG066831 (Menon) and U01AG072572 (De Jager/St George-Hyslop). This work was supported by grants from the National Institutes of Health (R01AG044546, P01AG003991, RF1AG053303, R01AG058501, U01AG058922, RF1AG058501 and R01AG057777). The recruitment and clinical characterization of research participants at Washington University were supported by NIH P50 AG05681, P01 AG03991, and P01 AG026276. This work was supported by access to equipment made possible by the Hope Center for Neurological Disorders, and the Departments of Neurology and Psychiatry at Washington University School of Medicine. We thank the contributors who collected samples used in this study, as well as patients and their families, whose help and participation made this work possible. This work was supported by access to equipment made possible by the Hope Center for Neurological Disorders, and the Departments of Neurology and Psychiatry at Washington University School of Medicine.

Table S2: Additional Taqman primers used in experiments, related to STAR Methods

Oligonucleotides	Source	Identifier
Dbp Taqman primer	ThermoFisher	Mm00497539_m1
Cd68 Taqman primer	ThermoFisher	Mm03047343_m1
Aif1 Taqman primer	ThermoFisher	Mm00479862_g1
Trem2 Taqman primer	ThermoFisher	Mm04209424_g1
Spp1 Taqman primer	ThermoFisher	Mm00436767_m1
Clec7a Taqman primer	ThermoFisher	Mm01183349_m1
Apoe Taqman primer	ThermoFisher	Mm01344172_m1
C1qa Taqman primer	ThermoFisher	Mm00432142_m1
C3 Taqman primer	ThermoFisher	Mm01232779_m1
Ccl2 Taqman primer	ThermoFisher	Mm00441242_m1
Cd22 Taqman primer	ThermoFisher	Mm00515432_m1
Cdkn2a Taqman primer	ThermoFisher	Mm00494449_m1
Ctsd Taqman primer	ThermoFisher	Mm00515586_m1
Cybb Taqman primer	ThermoFisher	Mm01287743_m1
Gbp2 Taqman primer	ThermoFisher	Mm00494576_g1
Gpnmb1 Taqman primer	ThermoFisher	Mm01328587_m1
Il1b Taqman primer	ThermoFisher	Mm00434228_m1
Il6 Taqman primer	ThermoFisher	Mm00446190_m1
Hmox1 Taqman primer	ThermoFisher	Mm00516005_m1
Lgals3 Taqman primer	ThermoFisher	Mm00802901_m1
Nlrp3 Taqman primer	ThermoFisher	Mm00840904_m1
Tgfb Taqman primer	ThermoFisher	Mm01178820_m1
Tnfa Taqman primer	ThermoFisher	Mm00443258_m1
Tyrobp Taqman primer	ThermoFisher	Mm00449152_m1